AIAA SciTech
4-8 January 2016, San Diego, California, USA
54th AIAA Aerospace Sciences Meeting

Development of the High Lift Common Research Model (HL-CRM): A Representative High Lift Configuration for Transonic Transports

Doug S. Lacy*
The Boeing Company,Boeing Commercial Airplanes, Seattle, WA, 98124

Anthony J. Sclafani.†
The Boeing Company, Boeing Commercial Airplanes, Long Beach, CA, 90846

The development of a high lift wing/body/nacelle/pylon/horizontal-tail configuration for a High Lift Common Research Model (HL-CRM) is presented. The high lift configuration includes inboard and outboard leading edge slats and inboard and outboard single-slotted flaps. Recommended nominal takeoff and landing positions are included for all devices. This geometry is based on a Common Research Model of a high speed configuration which has been the focus of many experimental and numerical studies throughout the world since 2008. Modifications of this prior geometry to enhance suitability for low speed purposes are outlined. The geometry has been evaluated in CFD through a range of takeoff and landing positions, and the results are discussed herein. Rationale for many of the decisions made during the design and positioning of the high lift devices is also provided. This effort was motivated by the lack of relevant high lift geometry available in the public domain that could be used to support collaborative efforts. It was modeled after the very successful efforts associated with the original CRM geometry referenced above. Planning efforts are already underway at NASA Langley Research Center to build a wind tunnel model based on the HL-CRM geometry as well as to use it as the basis for test cases to be assessed in future AIAA CFD High Lift Prediction Workshops.

* Aerospace Engineer, Product Development, PO Box 3707 MS 0R-120, Seattle, WA 98124, AIAA Senior Member.
† Aerospace Engineer, SoCal Design Center, 3855 Lakewood Blvd, Long Beach, CA 90846, AIAA Senior Member.

Nomenclature

CFD	=	computational fluid dynamics
CRM	=	common research model
C_D	=	drag coefficient, $Drag/(q_\infty S_{ref})$
C_f	=	skin friction coefficient
C_L	=	lift coefficient, $Lift/(q_\infty S_{ref})$
C_{le}	=	leading edge device chord, measured streamwise
C_M	=	pitching moment coefficient, $Moment/(q_\infty S_{ref} C_{ref})$
C_{ref}	=	wing reference chord
C_{te}	=	trailing edge device chord, measured streamwise
C_{wing}	=	wing chord, measured streamwise
QCR	=	quadratic constitutive relation
R_N	=	Reynolds number
RANS	=	Reynolds-averaged Navier-Stokes
S_{ref}	=	wing reference area
X	=	x-coordinate location, streamwise
Y	=	y-coordinate location, spanwise
WUSS	=	wing under slat surface
α	=	angle-of-attack
δ	=	device deflection

I. Introduction

The availability of geometry and high quality test data of relevant commercial transport high lift configurations in the public domain is very limited. Geometry and test data for current production aircraft is often held closely by their manufacturers for a variety of reasons. As such, available geometry usually falls into two categories: dated aerodynamics (e.g. wing or high lift device sections) on a relevant planform or potentially relevant aerodynamics on a planform not representative of a commercial transport (e.g. simple low aspect ratio trapezoidal wing). The current effort is aimed at filling this void by creating a set of relevant high lift geometry that can be made available in the public domain. It is envisioned that it will be used as the basis of wind tunnel testing efforts in the future to enable the generation of high quality data sets that can also be shared in the public domain. These could prove very useful in future Computational Fluid Dynamics (CFD) validation efforts such as the AIAA CFD High Lift Prediction Workshop.[1,2] It can also serve as a high lift technology development platform, with the performance levels achieved by the geometry serving as benchmarks for a conventional high lift system.

An additional objective of this effort was to create geometry that was easy to use. Issues can arise with geometry sets that are destined to be distributed amongst different Computer-Aided Design (CAD) systems, particularly with surfaces made up of multiple underlying surfaces. Generating a watertight surface from multiple pieces can sometimes present a challenge. Even maintaining object names through file transfers to different CAD systems is not assured. While these factors may not present many issues for a high speed model with its limited number of parts, they can for a high lift model which has many more surfaces and associated positioning and trimming information. Therefore, an attempt was made to provide the definition of each element as one surface element. In addition, thought was given as to how to best provide high lift device positioning and trim information within the CAD definition in a generic form that could be used in any CAD system.

The high speed CRM definition[3,4] provides a useful and logical springboard for this effort, as it is a wing/body/horizontal/nacelle/pylon geometry set representative of a generic long range, twin engine configuration. For this effort to produce a high lift geometry set, each high speed element was re-evaluated for its suitability for this role. For all elements, the goal was for the result to be representative of a modern commercial airplane, without including all of the details of a fully integrated design or the specific design approaches to accommodate them. In addition, given that this is to be used for research purposes and CFD validation, some design decisions were made to steer the geometry in the direction of spanwise consistency of some of the design variables (such as device gap) and overall geometric simplicity in the hopes of making it easier to interpret future CFD and testing results. Other constraints were imposed to help support a "building block" approach to assessing the geometry, starting with a wing/body configuration and adding complexity one step at a time (trailing edge flaps then leading edge slats then nacelle and pylon).

Lastly, while CFD was used to design and evaluate this geometry, it should be noted that these predictions only provided guidance for the effort. Obtaining reliable computational results for scenarios where accurate prediction of smooth surface separation is required is challenging, and the solutions are usually open to interpretation. In the end, it is expected that the surfaces and positioning provided herein offer a good starting point for a future wind tunnel test, and that with positioning adjustments representative takeoff and landing configurations can be established.

II. Geometry Development

A. Wing

While it was desired to maintain as much similarity to the existing high speed CRM wing geometry as possible, there were a number of issues that pointed to a re-lofting of the wing for high lift purposes:

- Spanwise straightening for easier implementation of high lift devices
- Leading edge curvature modifications to make more amenable to low-speed operation
- Desire for a one piece loft (modeling simplicity for wind tunnel and CFD)
- Desire for "wing reference system" loft definition

The original CRM wing was lofted from a list of planar design sections that were in constant Y planes in airplane coordinate system. These sections were sheared vertically such that a surface created through them represented a wing under cruise flight loading. Figure 1 shows the inherent "bending" in the CRM wing loft. While there is similar bending in low speed flight, defining high lift system parts in a wing with analogous bending would complicate the design, build and testing of wind tunnels models constructed from the geometry. Straightening the wing in a spanwise sense to something closer to the as-built shear distribution for a real airplane in an unloaded (tooling supported) position simplifies these downstream tasks. There are several options for how this can be achieved. One way is to simply pick a spanline on the upper or lower wing surface and force it to be a straight line. Choosing a spanline near the leading edge will tend to straighten the leading edge devices and keep spanwise distributions of variables like gap more uniform. However, straightening spanlines near the leading edge will force curvature into spanlines closer to the trailing edge, with corresponding effects on trailing edge device shapes and positioning. A spanline on the upper surface near the stowed slat trailing edge was utilized here. This simplified the design and positioning of the full span slats. The resulting curvature in the region of the trailing edge flaps was found to be manageable.

The original high speed CRM wing was created for high speed purposes only. Low speed operation was not a factor in its design. As a result, the leading edge has higher curvatures, particularly across the outboard wing, than would normally be present on a commercial transport which has been designed with both speed regimes in mind. While this can be dealt with in the design of the leading edge high lift system, there was a concern that this may lead to further non-representative features in the configuration. In the case of the slats utilized here, the higher cruise wing curvatures would mean higher slat leading edge curvatures which might require larger nose down deflections to make them work for the landing scenario. This would also likely impact the takeoff positioning. All of this would impact the Wing Under Slat Surface (WUSS) design.

In order to help keep the configuration more representative of existing designs, the decision was made to soften the cruise wing leading edge curvatures by increasing the effective leading edge radius of the defining wing sections. An example of the modification incorporated in the HL-CRM wing is shown in Figure 2. It should also be noted that the lower surface is flatter closer to the leading edge than before, making Krueger flap leading edge devices easier to integrate should there be a desire to do so in the future. Lastly, an additional sectional modification was made to set the trailing edge thickness to 0.20" full scale. This was done as part of an effort to make all potentially sharp element trailing edges a sufficient thickness at full scale to enable them to have adequate thickness at model scale. This 0.20" value should support wind tunnel model scales as low as 5-6% without resulting in model trailing edge thicknesses that are difficult to manufacture or lack robustness.

The original high speed CRM was defined as four surfaces, an upper and a lower surface for the inboard wing (inboard of the trailing edge planform break) and upper and lower surfaces for the outboard wing. As noted, all were lofted from chordwise airfoil sections defined in constant Y planes in the airplane coordinate system. This process of separating the loft into inboard and outboard portions eliminated the complexities associated with lofting across the mid-wing trailing edge planform break located at the outboard end of the yehudi, but it also resulted in spanline discontinuities across the junction to exist for the full chord. While these coincide with a natural flap span break on the trailing edge, they fall within the span of the outboard leading edge slats. For ease of design of these devices, a smooth, continuous wing loft for their full span was desired. In addition, many CFD processes expect a single surface wing as their input. Taking all of these factors into account, the decision was made to create a one piece wing loft. This was done such that constant parametric spanlines are curvature continuous over approximately the first 75% of the chord at the trailing edge break section of the wing, aft of which a discontinuity is allowed to phase in approaching the physical tangency break at the wing trailing edge. Given that it is anticipated that all of the parts in this aft region of any future wind tunnel model (e.g. flaps and spoilers) will have edges coincident with this discontinuity, no build issues should result. A comparison of the spanlines of the new one-piece loft and those of the high speed CRM sub-surfaces is presented in Figure 3.

For wing high lift devices, it is very useful to have geometry defined relative to a reference plane that is aligned with the wing. It is also easier to provide references to such a plane on wind tunnel models created from the geometry by, for example, aligning part interfaces with it. This plane is most easily created by defining a wing coordinate system where the Z=0 plane represents the wing reference plane, the X-axis is parallel to the airplane

coordinate system X-axis and on the body centerline (i.e., longitudinal axis) and the Y-axis deviates from the airplane coordinate system Y-axis by an effective dihedral angle. The overall objective was to define a straightened wing that was for the most part centered on the wing reference plane that when rotated by this angle around the X-axis and then translated an appropriate amount in airplane system X and Z would approximate the high speed CRM wing at the side of body and at the tip. Given that this "centering" is somewhat arbitrary, a round value of 5.0 degrees was chosen for the effective dihedral angle. The translations in airplane coordinates to move the rotated wing to the proper position in airplane coordinates are: dX = 899.92 inches and dZ = 163.50 inches. It should be noted that while this new wing loft is defined in wing coordinate system, it will be released in airplane coordinate system, for consistency, along with all other geometry information. The fact that the loft was already being adjusted in several ways for other reasons provided an opportunity to redefine it in the wing coordinate system, with defining airfoils in constant Y planes in this system, as opposed to the high speed CRM where they are in constant Y planes in body system. This will make a "geometrically cleaner" wing in which to do subsequent design work.

The wing planform in wing coordinate system, provided in Figure 4, was chosen such that the plan view definition of the new high lift wing loft would approximate that of the high speed CRM loft. They are not exactly the same due to the fact that the shearing and rotation of defining sections described above results in small changes in the planform. It should also be noted that the sections of the new loft have been scaled to match the defined wing reference system planform. Therefore, the new loft has a straight leading edge in plan view in wing coordinate system as well as two straight line trailing edge segments. (The high speed CRM loft did not strictly adhere to a straight line planform definition.)

To summarize, a new wing loft has been created through the following steps:

- Started with defining airfoils from the high speed CRM (twist distribution smoothed slightly)
- Airfoils modified near leading edge to reduce curvature
- Airfoils sheared to straighten spanline near slat trailing edge
- Airfoils redefined in wing coordinate system and scaled to "straight" planform that approximates that of high speed CRM
- One-piece surface created from airfoils in such a way as to maintain curvature continuity everywhere except near trailing edge break
- Spanlines of resulting loft smoothed slightly
- Wing tip end cap generated for completeness ("flattened" semicircular cross-section)

The result is a wing loft that is similar to, but not the same as, that of the high speed CRM.

B. High Lift Devices

The primary objective in the design of the high lift system for the High Lift Common Research Model is that the geometry be representative of that found on a modern commercial jet transport. The types of devices should be those commonly in use. Their sizing should be representative of that of devices on modern airliners. The positioning of the surfaces should be in the range of similar devices in use today. Finally, it is desired that the high lift performance be representative of modern jet transports as well.

While representative performance was desired, there were no specific numerical targets for parameters such as lift and drag. As this is an entirely new high lift configuration, one without the benefit of prior wind tunnel data, it is expected that some adjustments might be required to arrive at what might be considered final takeoff and landing positioning once it reaches a wind tunnel. As such, the use of CFD in guiding the design and validation of this geometry was less targeted on specific numbers such as C_{Lmax} and more directed at demonstrating reasonable aerodynamic results at the stated nominal positioning as well as providing room to tailor the aerodynamic outcome in the tunnel by changing the positioning of the current geometry. As will be discussed, other factors such as ease of modeling in CFD were also considered in choosing the present device positioning. While CFD was utilized throughout the design of the high lift devices, the CFD focus of this paper is on analysis of the final design, which will follow a discussion of the design constraints and decisions of the individual devices.

1) Leading Edge Devices

The primary leading edge device types in use on jet transports today are slats, rigid Kruegers, variable camber Kruegers and a simple drooped leading edge. For outboard wings (outboard of the nacelle), far and away the most common device is the slat, which is actuated forward and nose down to enable desired positioning relative to the Wing Under Slat Surface (WUSS), the designed main wing element leading edge surface that is covered by the slat when it is stowed for cruise. For inboard leading edges, more options have historically been utilized. However, slats

were chosen for the HL-CRM to enable full-span continuous leading edge configurations in the absence of the nacelle and pylon.

There were two objectives for the leading edge design. First was to enable the wing to reach sufficiently high angles of attack for takeoff and landing configurations to enable representative performance levels to be achieved. The second was for the airplane to pitch nose down at stall to aid in stall recovery. While that latter requirement has softened somewhat in modern transport design due to advances in electronic envelope limiting systems, it still seemed to be a noble goal for this configuration. Satisfying the first goal can be achieved through a combination of providing sufficient slat chord across the span and defining suitable slat positioning and WUSS designs. Satisfying the second goal requires one to manage the relative health of the inboard and outboard wing regions near stall. In order to get pitch down at stall, the inboard wing must stall first. There are a number of factors involved in making this occur, including slat chord distribution and slat positioning to be addressed here. Additional geometric features such as the presence of one or more nacelle chines (fan cowl mounted vortex generators), a leading edge strake at the side of body and/or different treatments of slat end. Some of these will be discussed later.

As stated above, it was desired to maintain a continuous leading edge chord distribution across the nacelle region in order to permit a reasonable nacelle/pylon-off configuration to be achieved. For simplicity, it was also desired to have linear distributions of chord both inboard and outboard of the nacelle. These desires coupled with an assessment of the range of chord versus span from a collection of existing airplanes led to the decision to choose a constant chord slat over the inboard span, and distribution of chord over the outboard span that tapers down linearly from the nacelle location to the wing tip. The final slat chord distribution is shown plotted with the range of slat sizing from previous airplanes in Figure 5.

Most transports configured with slats have at least two deployed positions, and two have been defined for the HL-CRM. The fully extended position is referred to as the landing position, while the intermediate position will be used for takeoff configurations. Many recent transports configured with slats employ a circular arc trajectory between the stowed and deployed positions. For enhanced realism, this has been used as a constraint for the HL-CRM as well. While it is possible to employ a different axis of rotation for each individual slat panel, a single axis has been defined for the whole inboard slat span and another axis has been defined for the entire outboard slat span. This was done for simplicity as well as to enable flexibility in possible future slat segmentation decisions. It should also be noted that both the takeoff and landing slat positions employ a gap between the slat upper surface trailing edge and WUSS. While this gap is zero (sealed) for some or all of the span at some positions for some in-service transports, a small gap is maintained across the entire span for takeoff and a larger one for landing for the HL-CRM. This was mostly done to ease grid generation for all of the initial configurations. However, the option of sealing remains for the wind tunnel should it be required for performance reasons.

There was an attempt to maintain as much realism in the constraints of the slat and WUSS surfaces as possible. A sufficient distance between the slat leading edge and the WUSS leading edge was maintained for structural viability reasons. In addition, the WUSS upper surface was designed assuming a thinner, more realistic slat trailing edge thickness. However the actual upper and lower slat trailing edge thicknesses have been opened up to 0.20" full scale for wind tunnel model viability by altering the inner slat cove surface. As a result, wind tunnel model slats built with these definitions cannot be stowed due to interference. (See Figure 6.) This is not deemed to be an issue as separate cruise leading edge parts can be built to test the stowed slat configuration.

Once all of the constraints are taken into account, the shape of the WUSS for a given slat span becomes fairly constrained. The main geometric variables in play boil down to: slat rotation axis, takeoff and landing rotations about that axis and shape of the WUSS. The slat gaps and heights for takeoff and landing as well as the pressure distributions on the slat and WUSS for both configurations are largely fallouts of these geometric inputs. While the shape of the pressure distribution on the slats is prescribed by the cruise wing shape, that of the WUSS can be managed through curvature manipulation. The relative loading between the two can be adjusted by changing the slat angle. Increasing slat angle decreases slat loading and increases loading on the WUSS.

Taking all of the constraints into account, along with the desire to maintain equal inboard/outboard slat angles to enable a clean nacelle and pylon removed configuration, a design solution consisting of inboard and outboard WUSS designs and slat rotation axes was found that positioned all of the slats at 30° for landing and 22° for takeoff. Further discussion of this recommended slat positioning can be found in the CFD analysis section later in this paper.

2) Trailing Edge Devices

While there are many different ways of configuring, supporting and actuating them, single-slotted flaps have become the norm for new commercial transport aircraft. Reduced complexity and weight, cost and lower noise are but a few reasons for this trend. Therefore, single-slotted flaps were chosen for the HL-CRM trailing edge. As with the leading edge, a distribution of device chord needed to be chosen, and as with the slats, device sizing from

existing jet transport airplanes was examined for guidance. Based on these data, flap chord across the outboard flap was chosen to be 25% of local wing chord. For the inboard flap, a constant chord across the span was chosen that was equal to the chord of the outboard flap at its inboard end. As can be seen in Figure 7, this chord distribution falls in the middle of the historical data. The other key variable to establish is the location of the spoiler-trailing-edge (or fixed-trailing-edge in regions of flap span without spoilers) relative to the flap. The further aft on the flap that this is, the more aft translation (fowler motion) that results as the flap deploys. The spoiler trailing edge was placed at 40% of flap chord for the HL-CRM, a value representative of typical commercial transports.

The chosen constraints result in a fair amount of flexibility in the shape of the pressure distribution that can be achieved. This flexibility can be used to pick a design philosophy to apply or provided as usable design space to an optimization framework. The design goal chosen for the HL-CRM was a consistent application of a generic triangular pressure distribution with a uniform spanwise gap distribution at the maximum landing flap angle of 40°. Due to the fact that the wing was sheared to produce straight upper surface spanlines in the vicinity of the stowed slat trailing edge, a fair amount of curvature in rear view exists in the curve representing the spoiler trailing edge, relative to which the flap gap is measured. This characteristic tends to drive the configuration toward non-linear spanwise gap distributions, with larger than desired gaps in the mid-span regions of the flaps. To combat this tendency, the stowed flap leading edge was pushed forward somewhat in the middle of both flap elements relative to the chord definition specified above. Through this chord modification and flap shape tailoring across the span, the design goal was achieved.

Given that there are many ways that single-slotted flaps can be supported and actuated on actual airplanes, a generic approach was taken to determining intermediate flap positioning for the HL-CRM, as opposed to picking some mechanism-specific constraints, e.g. the circular arc assumption imposed on the leading edge positioning. This involved making simplifying assumptions about how gap and overlap vary with deflection. These assumptions are shown in non-dimensional terms in Figure 8. For gap, they are expressed as gap over reference chord, which is defined as equal to the local wing chord across the outboard flap span and equal to the wing chord at the wing trailing edge break (constant) across the inboard flap span. The overlaps are expressed as a percentage of the difference in overlap from stowed to fully deployed. The desired overlap can be calculated by looking up the percentage as a function of deflection, multiplying this percentage, expressed as a fraction, by the difference between the overlaps of the stowed and fully deployed flaps and adding this amount to the fully deployed flap overlap. These relationships were used to determine the gaps and overlaps at the ends of the flap elements, which will help ensure alignment of the elements at the inboard/outboard flap junction.

The above approach requires an initial assumption for maximum landing flap angle. A value of 40° was chosen here. However, it is expected that multiple flap angles will be evaluated in CFD and in the wind tunnel as potentially better landing positions. It is suggested that the 40°gap and overlap values be used for all of them, so that the effects of angle, gap and overlap can be evaluated independently. It is also recommended that the initial nominal flap deflection for the inboard and outboard flaps be 37° for reasons that will be discussed in the analysis section below.

Pictures of the outboard flap in the 25° and 40° positions are shown in Figure 9. These show how the flap leading edge tracks the spoiler trailing edge to provide the uniform gap distributions. Plots of non-dimensionalized gap and overlap for a range of flap deflections for the inboard and outboard flap are shown in Figure 10.

Nacelle and Pylon

The high speed CRM was configured with a flow-through fan cowl that was attached to the wing with a pylon. The initial objective was to simply position this existing nacelle and pylon on the new wing for the HL-CRM using the same methodology as used to position it previously on the high speed CRM wing. While this is essentially what was done, a few modifications were made along the way.

First, it was determined that the pylon intersection with the wing lower surface extended aft onto the lower surface of the stowed flap. To simplify flaps down modeling, the pylon was shortened by 12 inches so that it closed out ahead of the stowed flap leading edge. The modification was all done aft of the point of maximum thickness of the pylon and is expected to have minimal effect on the aerodynamic performance at low speeds.

Next, the trailing edges of the pylon and the fan cowl were adjusted to 0.20” thick (full scale). For the pylon, this modification was also incorporated into the region aft of the maximum thickness. For the fan cowl, the inner cowl was modified to produce the desired trailing edge thickness.

Lastly, the surfaces for both cowl and pylon were approximated in such a way as to make them easier to use. For the cowl, this took the form of combining the inner and outer cowl surfaces into one simple surface. For the pylon, it was an effort to simplify a very detailed and complex surface. The original high speed CRM pylon had a complex topology and contained well in excess of two million patches. For the HL-CRM, complex portions of the surface that were inside the wing were trimmed away and the remaining surface was approximated. The result is a simpler

and much smaller (fewer patches) surface. The final nacelle cowl and pylon are shown in Figure 11 and 12, respectively.

C. Fuselage

The intent was to carry across the same fuselage definition from the high speed CRM to the HL-CRM. However, the original definition was a patchwork of approximately two dozen smaller surfaces. As it turned out, there were abutment issues between some of the surfaces that needed to be addressed to improve its usability in downstream CFD and wind tunnel model definition processes. For the high speed CRM, this work was done by various parties in ways to suit their particular needs. Unfortunately, some amount of configuration control was lost in the process.

For the HL-CRM, there were two potential paths which could be pursued. The first would be to declare an official version of the original patchwork that had all known issues addressed. The upside of this approach is that the result should be pretty consistent with the fuselage of the high speed CRM. One potential downside is that it is not assured that the processes of all potential users would be able to accept the patchwork definition. Under this scenario, the user would have to modify the geometry in a way to make it useful to them.

An alternative path would be to create a one-piece fuselage surface that was as close as possible to the original surface. Such a surface would most likely be usable in any downstream process without modification. Therefore, configuration control would be much easier to maintain. The downside is that the high speed CRM definition has "creases" present, most notably at the base of the windshield and around the junction of the wing-to-body fairing and the basic fuselage tube. Any process to "fit" a single surface would essentially be attempting to fit a smooth surface to something that isn't inherently smooth, which can lead to difficulties in these creased regions. An alternative would be to blend these creases in a controlled fashion over a limited area in their vicinity as part of the surface fitting process, resulting in deviations from the original definition.

In the end, the multi-patch route was preferred by the immediate downstream users of the geometry, those developing a wind tunnel model and those associated with near term meshing and CFD workshops. Therefore, the official fuselage definition for this geometry set is made up of multiple pieces. The surface topology is shown in Figure 13. A single piece version of the fuselage might be made available later for those who might need it. However, it should be noted that it would not be the same as the official version everywhere due to the required smoothing referred to above.

D. Horizontal Tail

The horizontal tail definition is essentially the same as that of the high speed CRM except that the trailing edge thickness has been modified to 0.20". A new tip cap was generated for this loft that is similar in character to the wing tip cap. All tail on cases were evaluated in the as defined, zero degree configuration.

III. CFD Analysis

Computational Fluid Dynamics (CFD) was used to estimate HL-CRM performance by exercising two trusted flow solvers: CFD++ and OVERFLOW. These are widely used RANS codes considered reliable and accurate for analyzing modern transport configurations at or near a design condition for both cruise and high-lift configurations. Evaluating general aerodynamic characteristics of the HL-CRM using two different methods allows for increased confidence that the overall design is generally acceptable. Both analyses started with the same geometry set which is an important requirement when attempting to compare results from different methods. The airplane configuration used for the code comparison includes the fuselage, slats, wing, flaps, nacelle and pylon. The results from this initial CFD assessment were close enough to allow for the continued use of a single code to explore effects of device positioning. A CFD++ analysis was performed with the horizontal tail included to evaluate multiple slat and flap deflections. General grid and solver information is briefly summarized below followed by a discussion of the results from both tail-off and tail-on analyses.

A. Grid Generation

Some details of the grids built for this analysis are provided for each method. The grids were constructed from scratch following best practices established from similar high-lift CFD studies. Given limitations on schedule, grid refinement effects were not explored.

1) CFD++

An unstructured mesh was built for the CFD++ analysis using a proprietary toolset which provides a degree of automation through several stages of the process. The automation offered by this toolset is one reason why CFD++

was selected over OVERFLOW for the slat/flap angle variation study. The high level of user experience with this unstructured grid generation process coupled with a deep experience base analyzing high-lift transport configurations meant that an established set of meshing guidelines and flow solver settings could be applied to this HL-CRM study and the results shared with confidence.

Unstructured volume grid generation was accomplished using a Boeing version of D. L. Marcum's Advancing Front/Local-Reconnection (AFLR) method[5]. The anisotropic tetrahedral mesh of the nominal takeoff configuration consists of 186 million cells and is shown in Figures 14 and 15. Following the previously mentioned best practices, careful attention was given to refining wake regions as shown in the first of these two volume grid images.

2) OVERFLOW

The HL-CRM structured, overset grid system was constructed under the general guidelines established for the 1st High Lift Prediction Workshop (HiLiftPW). Following the same grid generation process from HiLiftPW-1[6,7] and HiLiftPW-2[8], construction can be characterized by four general steps. In the first step, surface grids are built directly on the CAD definition using a Boeing-developed program called MADCAP which can import geometry from different file types (e.g. IGES). The second step is to export the surface grids out of MADCAP and use a script system[9] developed at NASA which is intended to work with the Chimera Grid Tools (CGT) package[10]. This script system brings a degree of automation to the overall process by defining boundary conditions for each grid, organizing components with a master configuration file, and driving the CGT programs with a master input file. A script tool called BuildVol generates volume grids where surface grids are run through one of two hyperbolic grid generators (HYPGEN[11] and LEGRID) and Cartesian box grids are created using a code called BOXGR. In the third step, a program called PEGASUS5[12] is used to establish communication between the individual volume grids or zones. This is a step in the process known as domain or grid connectivity. The zones are connected by cutting holes where points fall inside geometry or where another grid is found to have better spacing. At grid and hole boundaries, PEGASUS5 creates interpolation stencils which are needed to pass information across zones. The last major step in the overset grid generation process is needed to create a force and moment integration surface. This is accomplished using another Boeing program called POLYMIXSUR which is similar in function to NASA's MIXSUR program. These programs eliminate grid overlap on the surface and connect neighboring zones with zipper grids comprised of triangles to form a water tight surface for pressure integration which is used to compute forces and moments.

The surface grid topology for the landing configuration is shown in Figure 16. This image is intended to illustrate the general layout of the various grids that define the major airplane components such as the flaps. The geometry in this figure is defined by the surface mesh which, in some areas, is so dense it appears to be a solid surface. The grid is made-up of 86.6 million points which is comparable to the HiLiftPW-2 grid built for a similar model of a transport configuration designated DLR-F11.[13] The F11 grid for the medium mesh level had 69 million points which is consistent with the grid density of the HL-CRM because the F11 grid did not include a nacelle/strut and the slat and flap were one-piece surfaces which means fewer end cap grids. It is important to note that the wake portion of the surface abutting grids is not shown in Figure16. A sense of how wakes were modeled may be given in Figure 17 which shows a planar slice through the volume grid in the mid-span wing region. Close inspection of the images in this figure reveals the relative spacing and extent of the slat, wing and flap wakes in the final mesh after holes have been cut and optimal overlap defined by PEGASUS5.

B. Flow Solver and Computing Platform

There are often as many ways to run a state-of-the-art RANS flow solver as there are machine types to run it on which is why it is important to clarify the approach used in these areas whenever CFD results are published.

1) CFD++

CFD++[14] is a widely used general purpose RANS code that is compatible with both structured and unstructured grids including overset and hybrid. Its finite volume solver for the steady/unsteady, compressible/incompressible Navier-Stokes equations can be applied to a large range of vehicle geometry and speed regimes. Multiple turbulence models are available as well as large-eddy simulation capabilities including hybrid RANS/LES models. The approach used for this HL-CRM analysis includes the use of low-Mach pre-conditioning, the one-equation Spalart-Allmaras turbulence model with rotation and curvature corrections (SARC) and the Quadratic Constitutive Relation (QCR) turned-on with the CR1 coefficient set to 0.35. These particular solver settings are aligned with the OVERFLOW setup described below.

2) OVERFLOW

OVERFLOW[15,16] is a node-based RANS code specifically designed for structured, overset grid systems. It is capable of computing steady or unsteady flow about an arbitrary body across a wide range of Mach numbers using a number of different approaches. Depending on the type of simulation, the solver can be run in 2D or 3D, thin-layer or full Navier-Stokes, central or upwind differencing and static or moving body. Other options available to the user are automatic mesh refinement and a number of different turbulence models including hybrid RANS/DES. A list of solver options exercised for the HL-CRM analysis is provided below.

- HLLE++ upwind flux method
- SSOR implicit solver
- TLNS3D dissipation scheme
- van Albada limiter
- low Mach pre-conditioning off
- 3rd order spatial accuracy
- global multi-grid off
- DT = 0.1, CFLMIN = 5.0
- Spalart-Allmaras turbulence model with rotation and curvature corrections (SA-noft2-RC)
- Quadratic Constitutive Relation (QCR), CNL1 = 0.35

OVERFLOW version 2.2g was run in parallel using the Message Passing Interface (MPI) libraries on a Linux PC cluster consisting of 2928 cores on 648 general compute nodes of mixed type. The type utilized for this analysis is a dual Intel 8-core 2.6 GHz 64-bit processors with 64GB of memory (4GB/core). The grid built for the nominal landing configuration (86.6 million points) was run on 96 cores or 6 nodes for 132 hours at a rate of 7.9 seconds per iteration. This translates to roughly 5 days of running for most cases, but angles-of-attack at the low and high ends of the lift curve required additional time to reach convergence. The solution convergence criteria used for this study is based on tracking the value of total lift coefficient. If there is no change in the mean value of lift to the third decimal place over the last several thousand iterations, then full convergence is achieved. Residual convergence characteristics will be discussed in the Results section.

C. Results

Results from the CFD++ and OVERFLOW analyses are summarized for multiple HL-CRM configurations. All simulations were made in free-air with a fully turbulent boundary layer. The free-stream Mach number was 0.2 and Reynolds number 24.6 million based on the mean aerodynamic chord. Additional runs are planned at a lower Reynolds number to predict performance levels and trends that may be measured during a wind tunnel entry but that analysis could not be completed in time for this paper.

The focus of these analyses was not to determine an exact value of C_{Lmax} for any particular configuration, but rather to determine whether the geometry and chosen final positioning were reasonable and produced results that are representative of a transport aircraft. As such, a complete "optimization" via CFD was not attempted. Instead, the focus was on:

- Are the results believable?
- Are the results reasonable/representative?
- Are the configurations robust?

The believability aspect was addressed through the use of two trusted, yet quite different, CFD codes. If results of similar character could be obtained from both, some confidence could be gained that what is being depicted by the codes is real, in spite of the challenges that the cases present. In regards to reasonable and representative results, the goal is to produce configurations that appear to stall at a representative angle of attack, through a representative stall mechanism with resulting representative pitching moment characteristics. In terms of robustness, the goal was to ensure that the nominal positioning did not put the configuration near a performance "cliff," where small changes in device shape or positioning might dramatically change the performance. If all of these areas can be addressed in a satisfactory way, there is a good probability of achieving success in an initial wind tunnel entry, where it is expected that a more thorough positioning study will be conducted.

1) Convergence Characteristics and Initial Conditions

Achieving reasonable flow solver convergence characteristics for a high-lift simulation can be challenging, particularly at high angles-of-attack. The convergence behavior for both flow solvers was verified to be consistent with similar analyses and accepted as reasonable for engineering purposes such as computing lift increments at operational angles-of-attack. Force, moment and residual convergence from an OVERFLOW solution of the nominal landing case is shown in Figure 18. All geometries and alphas analyzed exhibited some amount of oscillation in the force and moment convergence history as indicated in the figure. This was addressed by using a

mean value taken over the last 2000 iterations which typically varied by less than 0.001 in C_L once the solution was deemed "converged."

Flow solver residual convergence is given in the lower right plot of Figure 18 for the 6° angle-of-attack solution. This plot shows convergence levels for the various overset grid zones where the coarser box grids exhibit the worst residual convergence with a drop of 5 orders of magnitude while other zones converge to a much lower level with a drop of 10 orders of magnitude. This wide spread in residual convergence is typical for a high-lift OVERFLOW solution on a complex three-dimensional configuration.

It has been shown in the High Lift Prediction Workshop series that some RANS flow solvers produce multiple solutions for a given geometry/grid when the initial condition is changed from free-stream quantities to a prescribed flow field computed at a lower angle-of-attack. The HL-CRM is no exception for the CFD++ analysis where restarting the solver from lower angles-of-attack resulted in a higher lift level compared to free-stream initial conditions near stall. However, the trends were similar between the two approaches, and thus, both were deemed sufficient for the goals of this exercise cited above. Therefore, the CFD++ cases presented here were run from freestream for expediency. OVERFLOW did not have any initial condition dependency, so all of those cases were started from free-stream conditions as well.

2) Tail-off Nominal Slat/Flap Deflections

The nominal slat and flap deflections were analyzed for both takeoff and landing cases using CFD++ and OVERFLOW with the horizontal tail-off. The nominal takeoff slat and flap deflection is 22° and 25°, respectively. The corresponding landing deflections are 30º and 37º.

A comparison of computed lift curves is provided in Figure 19 where the CFD++ data is plotted as blue, solid lines and the OVERFLOW data as red, broken lines. Takeoff results have a square symbol and landing a triangle. The takeoff results for both codes are in good agreement up to an angle-of-attack of 14º. Between 14º and 17º, the methods differ on stall prediction with CFD++ showing a break in the lift curve at 16º while OVERFLOW data breaks at 17º. Discrepancies at or near stall are expected as modeling the complex flow physics of a high-lift system at high angles-of-attack is known to push the limits of RANS methods where variables such as mesh density and turbulence modeling can be strong drivers for the solution. A similar comparison is shown for the landing configuration but with more discrepancy through the linear portion of the lift curve where OVERFLOW predicts roughly 0.05 higher C_L. Overall, the code-to-code lift comparison is reasonable and offers some reassurance that the high-lift design is operating at representative levels with tail-off landing C_{Lmax} in the neighborhood of 2.3 to 2.4.

Figures 20 and 21 are drag and pitching moment comparisons for the nominal cases. The drag polars are in good agreement and show expected trends with reduced drag levels at operational angles-of-attack for the takeoff deflections. The predicted tail-off pitching moment curves show that CFD++ data are more nose-down for takeoff and more nose-up for landing compared to OVERFLOW at a given lift level. While the more nose down results for OVERFLOW at landing could likely be explained by more effective flaps relative to CFD++ (which would also explain the improved lift), no explanation has yet been found for the takeoff differences. Both methods show a strong nose-down pitch break at stall which is a good indicator of a representative design.

Upper surface streamlines and skin friction contours are provided in Figures 22 and 23 to show where flow separation initiates for the takeoff and landing configurations. Both CFD++ and OVERFLOW predict the same flow mechanism limiting C_{Lmax}: large-scale separation directly behind the nacelle. This is encouraging because a well designed nacelle chine can be used to delay separation and increase maximum lift as long as lift breakdown occurs on the inboard wing ensuring a nose-down pitch break.

3) Tail-On Slat/Flap Deflection Study

The tail-off results showed that the stall was dominated by separation behind the nacelle and not by overloading of the slats or WUSS's. However, it was desired to make sure that this was the case over a range of slat positions, to make sure that another region did not become limiting. Here, both the inboard and outboard slat angles were independently varied for both takeoff and landing. This was accomplished by rotating them +/-3 degrees around their trailing edges while in their design nominal positions. Therefore, slat height and gap were essentially unchanged. The six degree spread in angle enables the performance sensitivity to be evaluated over a significant change in relative loading between the slat and WUSS.

Results for the takeoff study are presented in Figure 24. The left side shows the impact of varying inboard slat angle on lift and pitching moment, and the right side shows the analogous impact of varying outboard slat angle. The C_{Lmax} varies only slightly amongst all of the cases owing to the limitation behind the nacelle. Decreasing the inboard slat angle appears to weaken the overall leading edge while decreasing the outboard slat angle strengthens it slightly.

A similar dataset for the landing configuration is shown in Figure 25. These data show more sensitivity to slat angle than for takeoff. While again, the C_{Lmax} varies only slightly amongst all of the cases owing to the limitation behind the nacelle, the angle of attack at which the lift curve breaks lower is increased as slat angle is increased, for both inboard and outboard slats. This further indicates the potential for a greater C_{Lmax} to be achieved should the nacelle region be addressed. It also appears to verify that differential inboard-outboard slat angles could be used to tune pitch characteristics should the need arise.

Finally, the impact of flap angle on landing performance was evaluated in CFD++. Four streamwise flap angles were evaluated: 34°, 37°, 40° and 43°. The angles were the same for both the inboard and outboard flaps for all cases, i.e. no differential inboard-outboard angles were evaluated. The lift, drag and moment results are shown in Figure 26. The lift curves in the lower left plot show steadily increasing lift with flap angle up to 40°, and essentially no additional gain for increasing to 43°. Results at C_{Lmax} are less clear, but it is fair to say that at 43°, the outboard flap is beyond its optimum angle. Results presented earlier indicate large scale separation on that flap at even 37°. This is likely hurting outboard wing performance as evidenced by the slight nose up moment trend near stall. Pitching moment through the linear lift region tracks with lift performance, as expected. Drag trends are also logical, with drag stepping up fairly uniformly with flap angle up to 40°. A larger drag increment is produced when increasing flap angle to 43°, as the system is not producing more lift, just more separation.

IV. Conclusions and Future Work

A High Lift Common Research Model geometry set has been developed based on the current high speed CRM. A leading edge system incorporating inboard and outboard slats has been designed, and representative takeoff and landing positions have been identified. A trailing edge system incorporating single-slotted flaps has also been designed and a range of takeoff and landing flap positions have been defined. Through this effort, the initial objective to create generic high lift configuration geometry that is representative of a commercial jet transport has been met.

A few configurations of the geometry have been evaluated using two RANS solvers, CFD++ and OVERFLOW, with similar results produced by both. A wider range of leading and trailing edge positioning was subsequently evaluated with CFD++. Results show`high lift performance levels representative of a commercial jet transport. The mechanism for stall initiation for all cases evaluated was a large scale separation on the wing behind the nacelle.

It was originally anticipated that a nacelle chine would be required to recover performance lost in this nacelle region, as this is typically the case. However, reasonable stall angles of attack were achieved without it, likely due to a nacelle placement that is not as close-coupled with the wing, which enables the slats to extend closer to the nacelle pylon than on some recent airplanes. However, it is highly recommended that an array of chine options (sizes and positioning) be developed for testing in the first wind tunnel entry, as the configuration likely is not reaching its full potential without one.

Clearly, inboard and outboard slat positioning (angles as well as gap and height distributions) represent additional "knobs" that can be turned to tune high angle of attack behavior. It is recommended that the wind tunnel model be configured to enable such adjustments. It the health of the region behind the nacelle is improved, it is quite possible that changes to the inboard slat positioning (e.g. gap reductions) will be required to ensure that the inboard wing breaks down before the outboard.

It should also be noted that the geometry currently does not have a strake the blends the wing leading edge into the body, which can also be a factor in premature stall. Again, reasonable stall angles have been achieved without one. However, the inboard trim of the inboard slat has been located in such a way as to allow one to be incorporated without altering the current slat geometry. Additional options are possible with slat extensions. It is recommended that the wind tunnel model be architected to allow the incorporation of strake options.

While any or all of the above adjustments may be required to arrive at the final takeoff and landing performance, it is recommended that the current 22° and 30° positioning remain the nominal takeoff and landing leading edge configurations at present.

For the trailing flaps, only a higher takeoff angle and a range of landing angles have been explored in CFD thus far. It is suggested that all of these angles and at least one lower takeoff angle be achievable in the tunnel, along with possibility of varying flap gap and overlap for each. While the landing performance was better at the 40° flap angle, it is suggested that the 37° angle carry forward as the current nominal. It's a better behaved configuration that is likely better suited for initial CFD studies that will inevitably utilize the nominal positioning.

While the geometry discussed in this paper enables basic high lift configurations to be assembled, there are some additional items that should still be defined. Some of these items should be defined in the near term so that the

planned wind tunnel half model can be designed to include them. These include main landing gear, ailerons and spoilers. Longer term a nose gear should be defined as well as a vertical tail.

V. Acknowledgments

The authors thank the National Aeronautics and Space Administration and The Boeing Company for supporting the development of the HL-CRM. Special thanks to the following individuals for their significant contributions to the design and analysis of the HL-CRM:

- Eric Dickey (Boeing Research and Technology)
- Bonnie Smith (Boeing Commercial Airplanes)
- Warren Burggraf (Boeing Commercial Airplanes)

The authors also thank a number of other Boeing contributors who helped to make the HL-CRM geometry development a success including John Vassberg, John Winkler, Neal Harrison, Pichuraman Sundaram, David Yeh, Lie-Mine Gea, Peter Hartwich, Greg Wyatt, Paul Vijgen and Dean Hawkinson.

References

[1]Rumsey, C., Slotnick, J., Long, M., Stuever, R., Wayman, T., "Summary of the First AIAA CFD High-Lift Prediction Workshop," Journal of Aircraft, Vol. 48, No. 6, pp. 2068-2079, November-December 2011.

[2]3rd AIAA CFD High Lift Prediction Workshop, URL: http://hiliftpw.larc.nasa.gov/, email: hiliftpw@gmail.com, June 2015.

[3]Vassberg, J.C., DeHaan, M.A., Rivers, S.M., Wahls, R.A., "Development of a Common Research Model for Applied CFD Validation Studies," AIAA Paper 2008-6919 (Invited), AIAA Applied Aerodynamics Conference, Honolulu, HI, 19 August 2008.

[4]NASA Common Research Model, URL: http://commonresearchmodel.larc.nasa.gov/, February 2012.

[5]Marcum, D. L., "Efficient Generation of High Quality Unstructured Surface and Volume Grids," Proceedings, 9th International Meshing Roundtable, Sandia National Laboratories, pp. distributed at conference, October 2000.

[6]Sclafani, A. J., Slotnick, J. P., Vassberg, J. C., Pulliam, T. H., Lee, H. C., "OVERFLOW Analysis of the NASA Trap Wing Model from the First High Lift Prediction Workshop," AIAA Paper 2011-0866, 49th AIAA Aerospace Sciences Meeting, Orlando, FL, January 2011.

[7]Sclafani, A. J., Slotnick, J. P., Vassberg, J. C., Pulliam, T. H., "Extended OVERFLOW Analysis of the NASA Trap Wing Wind Tunnel Model," AIAA Paper 2012-2919, 30th AIAA Applied Aerodynamics Conference, New Orleans, LA, June 2012.

[8]Pulliam, T. H., Sclafani, A. J., "High-Lift OVERFLOW Analysis of the DLR-F11 Wind Tunnel Model," AIAA Paper 2014-2697, 32nd AIAA Applied Aerodynamics Conference, Atlanta, GA, June 2014.

[9]Nash, S. M., Rogers, S. E., "Manual for Scripts," URL: http://rotorcraft.arc.nasa.gov/cfd/CFD4/CGT/scripts.html, January 2008.

[10]Chan, W. M., Rogers, S. E., Pandya, S. A., Kao, D. L., Buning, P. G., Meakin, R. L., Boger, D. A., Nash, S. M., "Chimera Grid Tools User's Manual," URL: http://people.nas.nasa.gov/~wchan/cgt/doc/man.html, Version 2.1, March 2010.

[11]Chan, W. M., Chiu, I. T., Buning, P. G., "User's Manual for the HYPGEN Hyperbolic Grid Generator and the HGUI Graphical User Interface," NASA TM 108791, October 1993.

[12]Suhs, N. E., Rogers, S. E., Dietz, W. E., "PEGASUS 5: An Automated Pre-processor for Overset-Grid CFD," AIAA Paper 2002-3186, 32nd AIAA Fluid Dynamics Conference, St. Louis, MI, June 2002.

[13]Rudnik, R., Huber, K., Melber-Wilkending, S., "EUROLIFT Test Case Description for the 2nd High Lift Prediction Workshop," AIAA 2012-2924, 30th Applied Aerodynamics Conference, New Orleans, Louisiana, June 2012.

[14]Chakaravathy, S., "A Unified-Grid Finite Volume Formation for Computational Fluid Dynamics," International Journal for Numerical Methods in Fluids, 31:309-323.

[15]Nichols, R. H., Buning, P. G., "User's Manual for OVERFLOW 2.2," URL: http://overflow.larc.nasa.gov/home/users-manual-for-overflow-2-2, Version 2.2k, March 2015.

[16]Nichols, R. H., Tramel, R. W., Buning, P. G., "Solver and Turbulence Model Upgrades to OVERFLOW 2 for Unsteady and High-Speed Applications," AIAA Paper 2006-2824, 25th Applied Aerodynamics Conference, San Francisco, CA, June 2006.

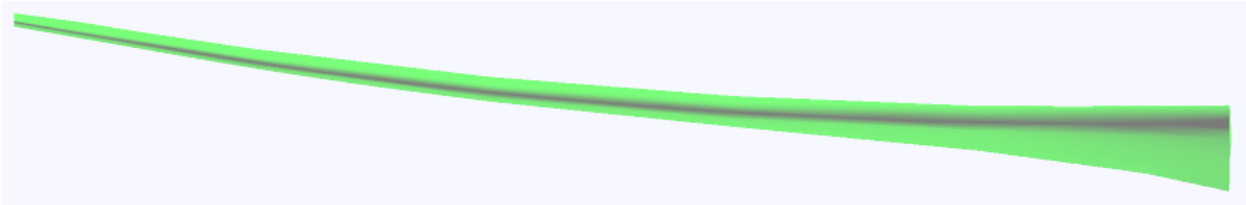

Figure 1. Front view of High Speed CRM wing showing bending.

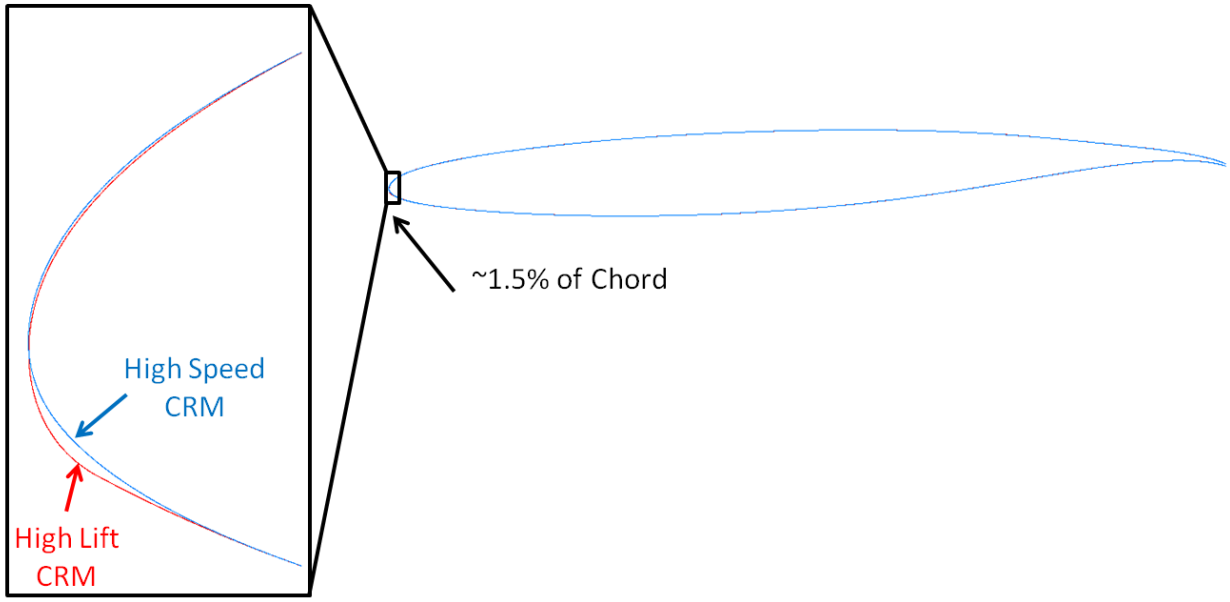

Figure 2. Example of leading edge curvature modification done to high speed CRM wing sections.

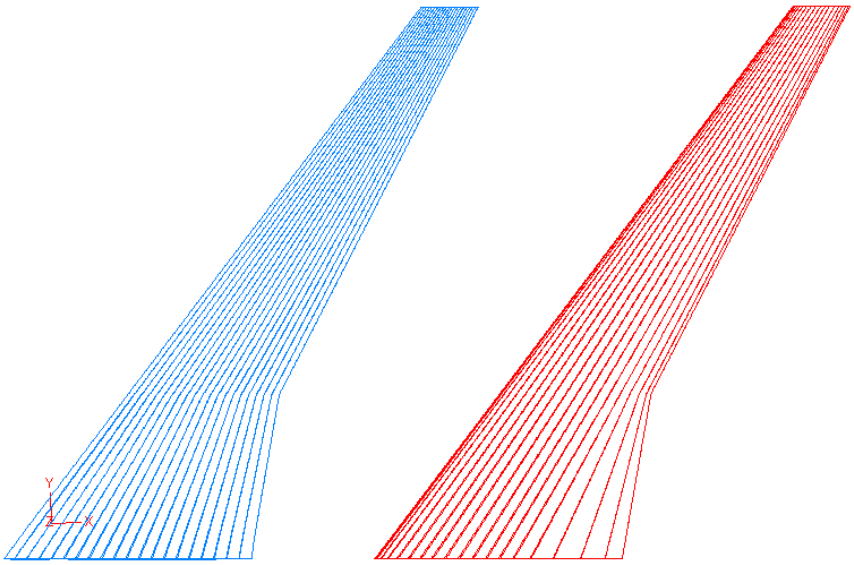

Figure 3. Comparison of high speed CRM spanlines (left) with high lift CRM spanlines (right).

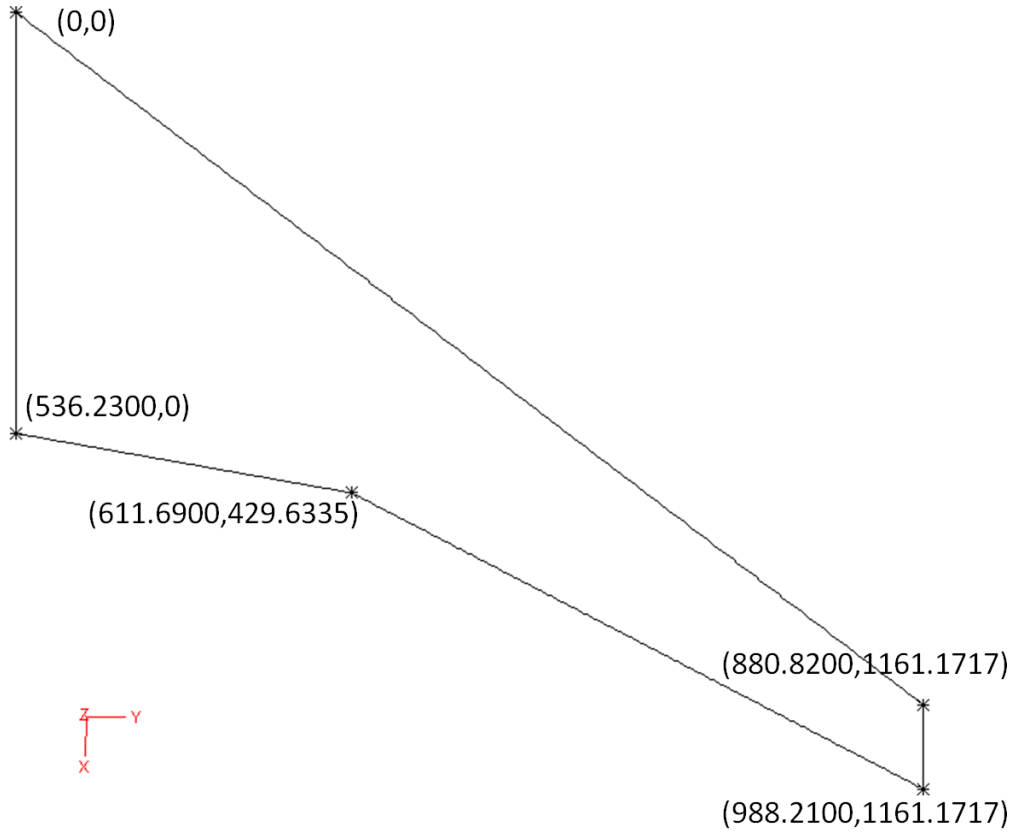

Figure 4. Wing planform in wing coordinate system.

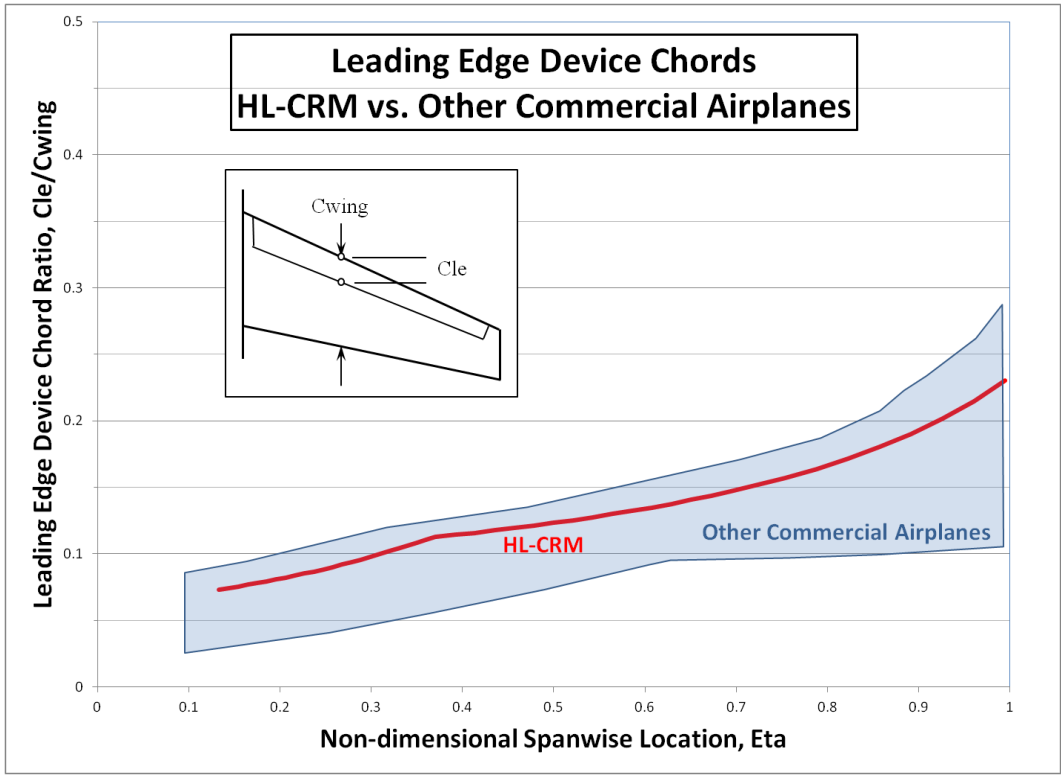

Figure 5. Non-dimensionalized HL-CRM leading edge chords relative to other commercial airplanes.

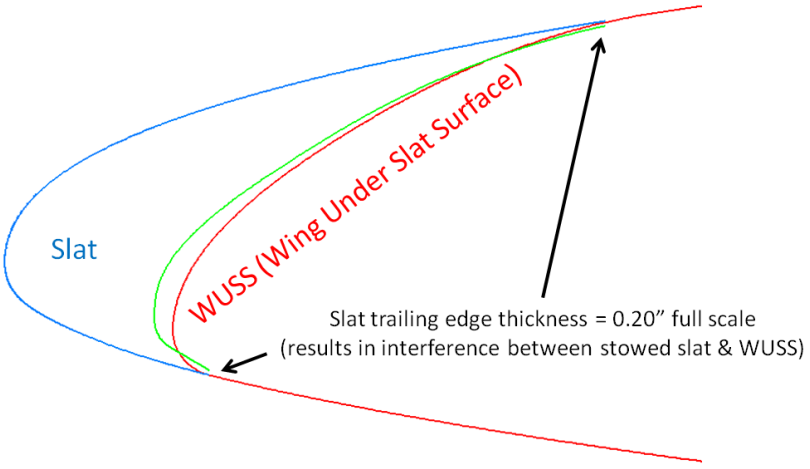

Figure 6. Cross section of outboard slat and WUSS.

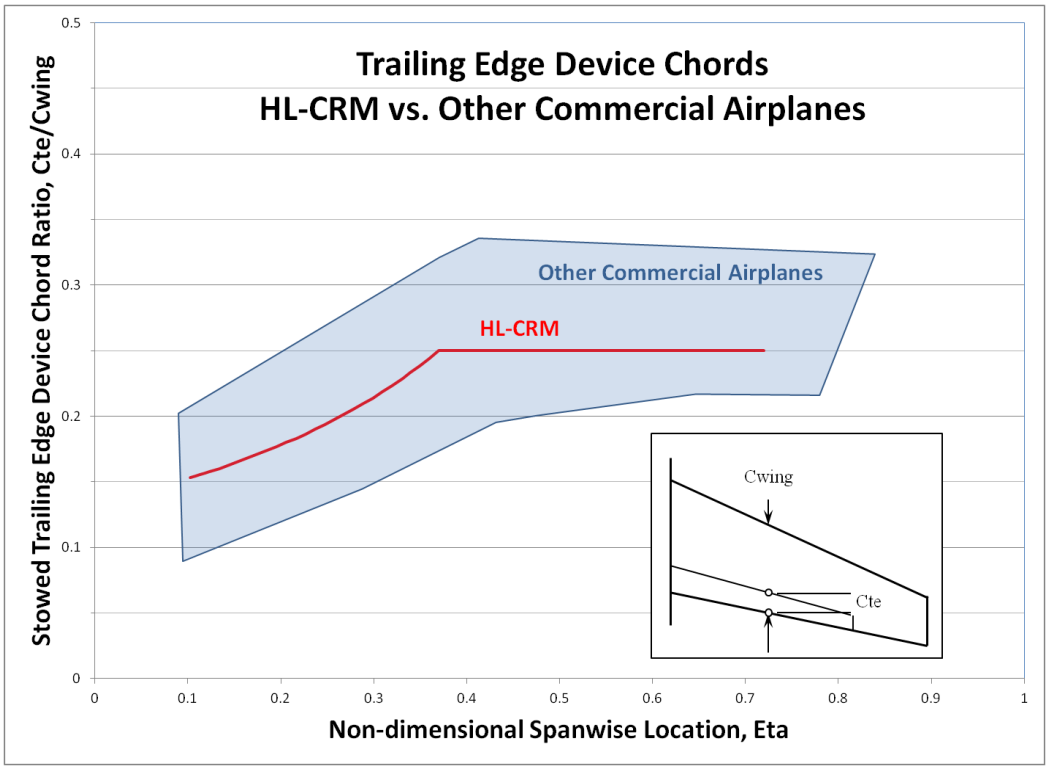

Figure 7. Non-dimensionalized HL-CRM leading edge chords relative to other commercial airplanes.

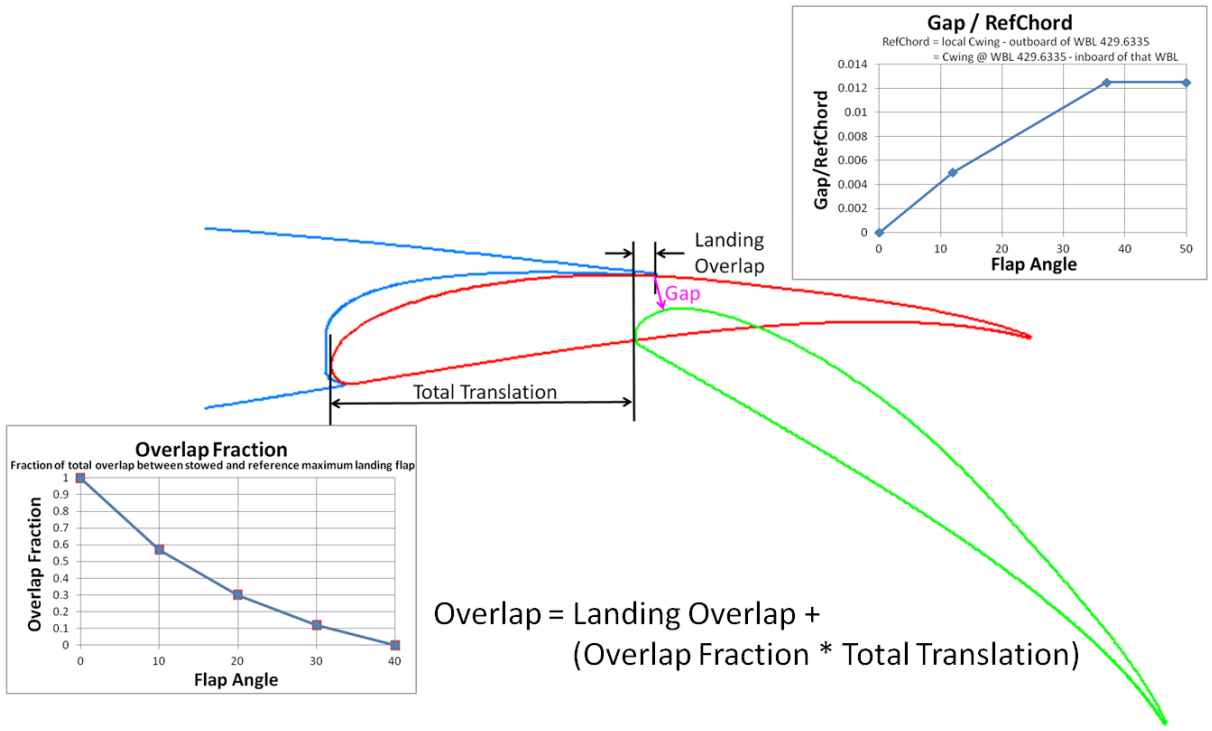

Figure 8. Flap positioning guidelines.

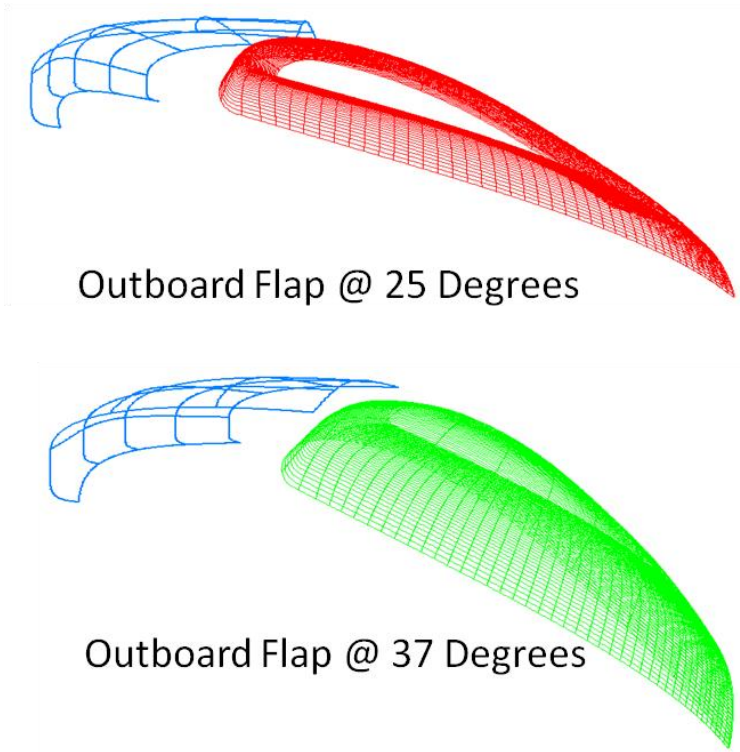

Figure 9. Positioned outboard flap.

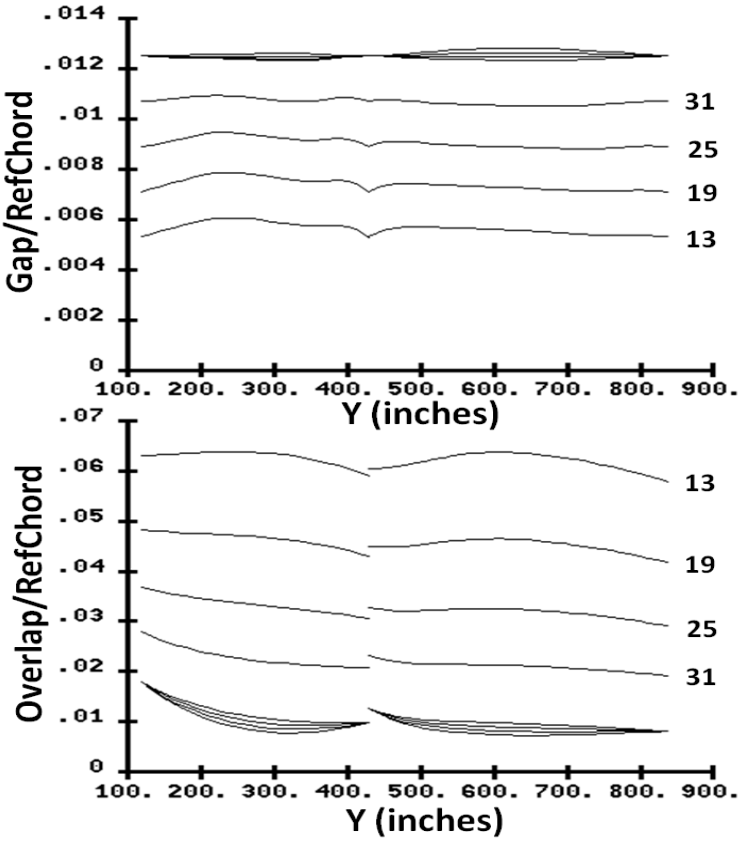

Figure 10. Non-dimensionalized inboard and outboard flap gaps and overlaps.

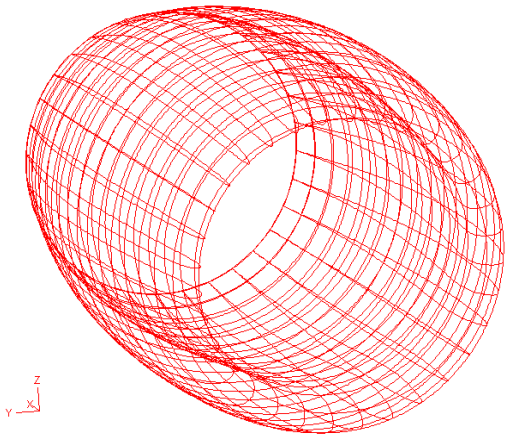

Figure 11. Nacelle Cowl.

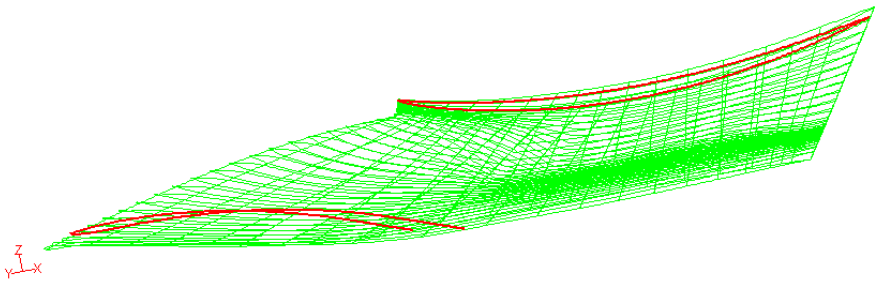

Figure 12. Nacelle pylon. (Cowl/wing intersections in red.)

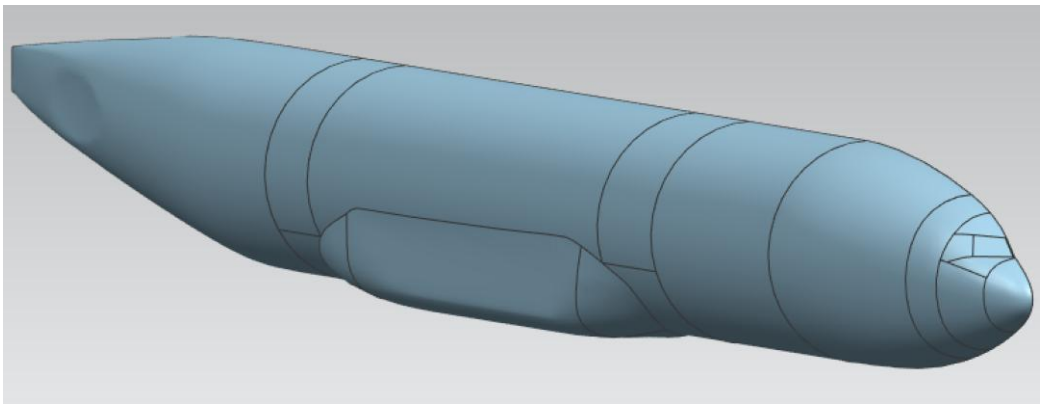

Figure 13. Multi-patch fuselage definition.

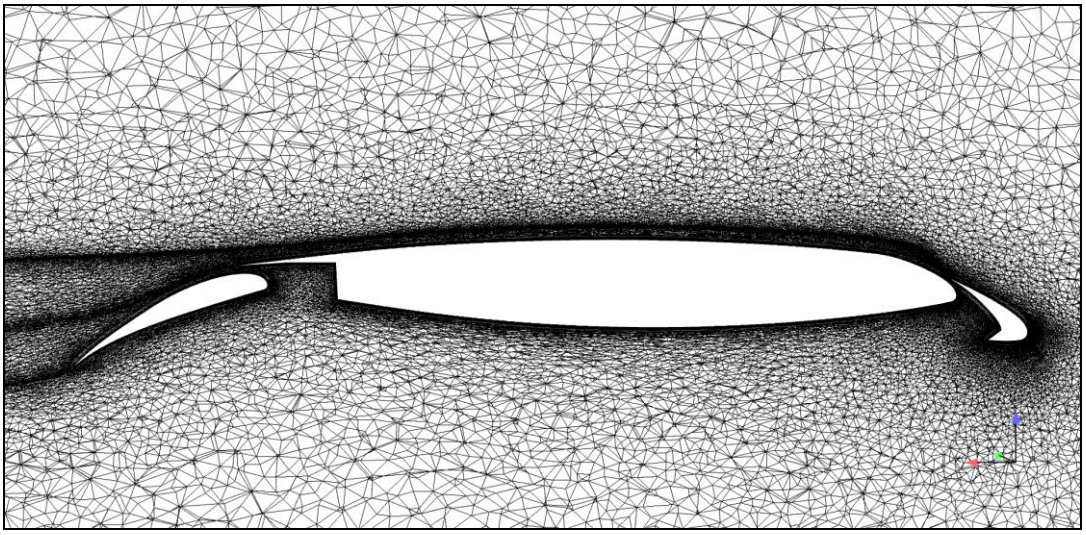

Figure 14. Anisotropic tetrahedral nosh of takeoff configuration.

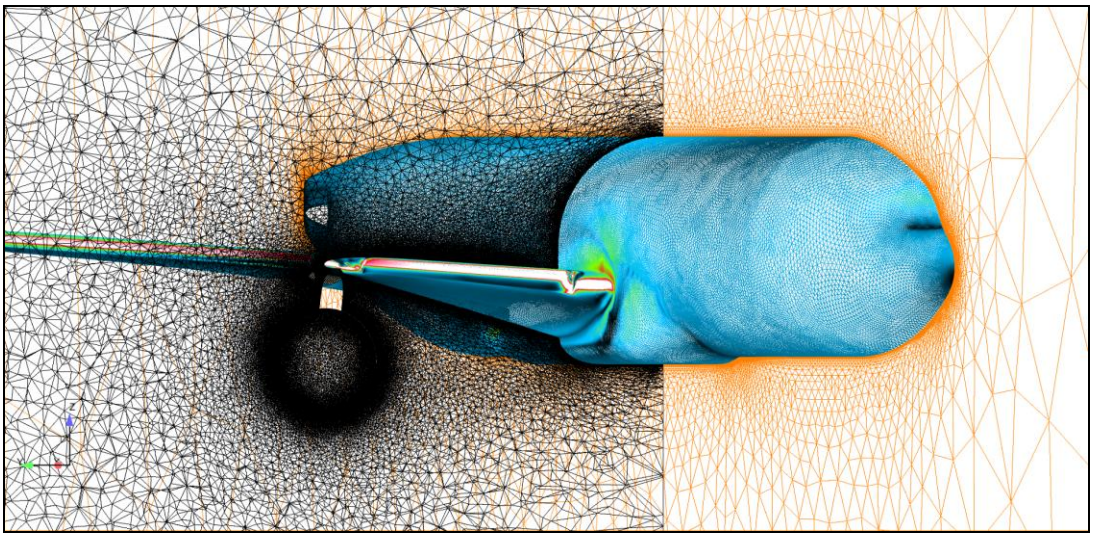

Figure 15. Anisotropic tetrahedral mesh of takeoff configuration.

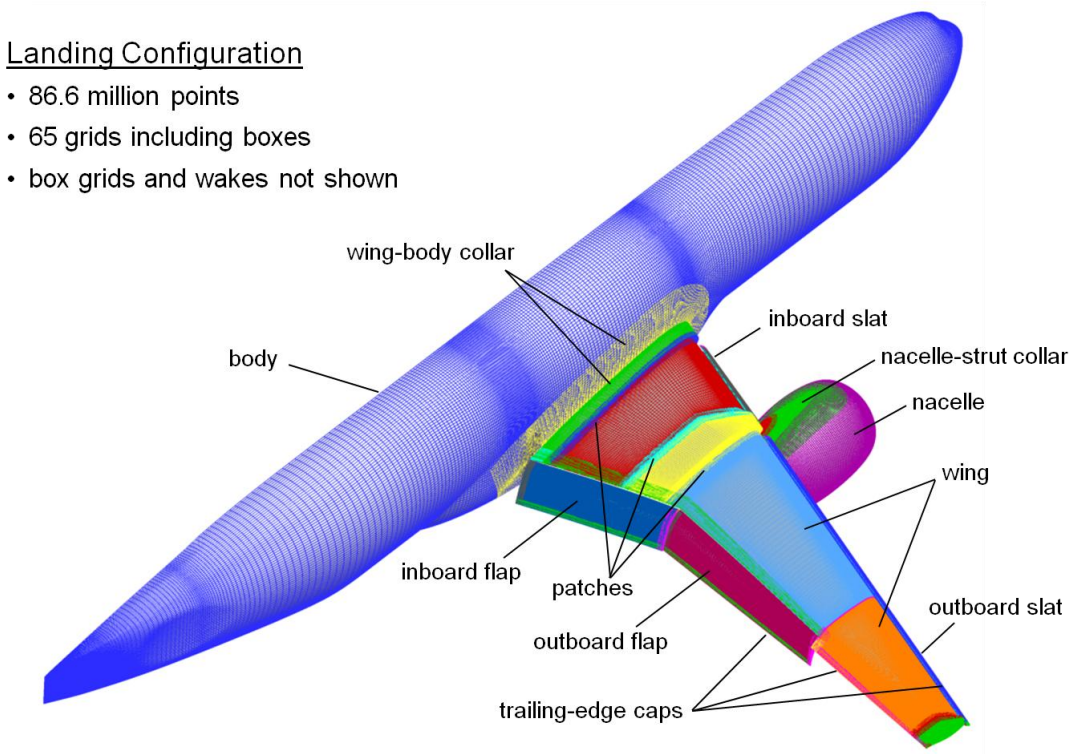

Figure 16. OVERFLOW surface grid topology.

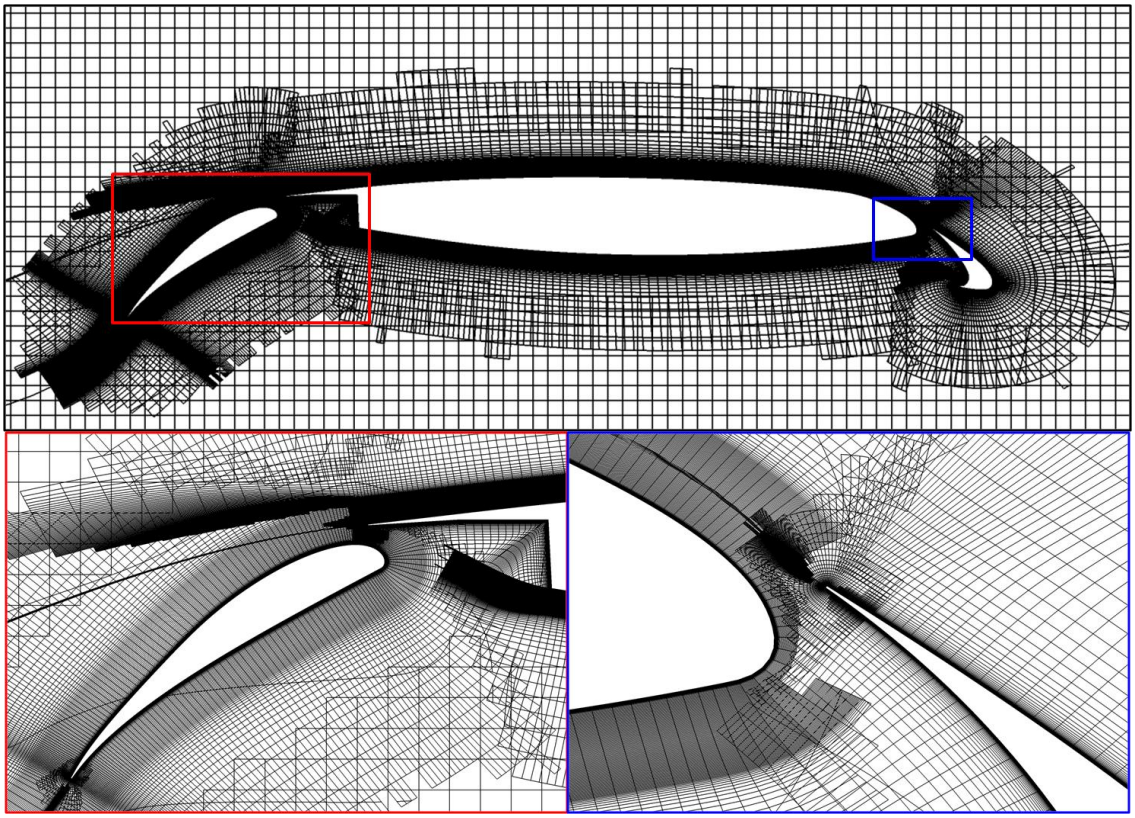

Figure 17. OVERFLOW volume grid, mid-span wing slice.

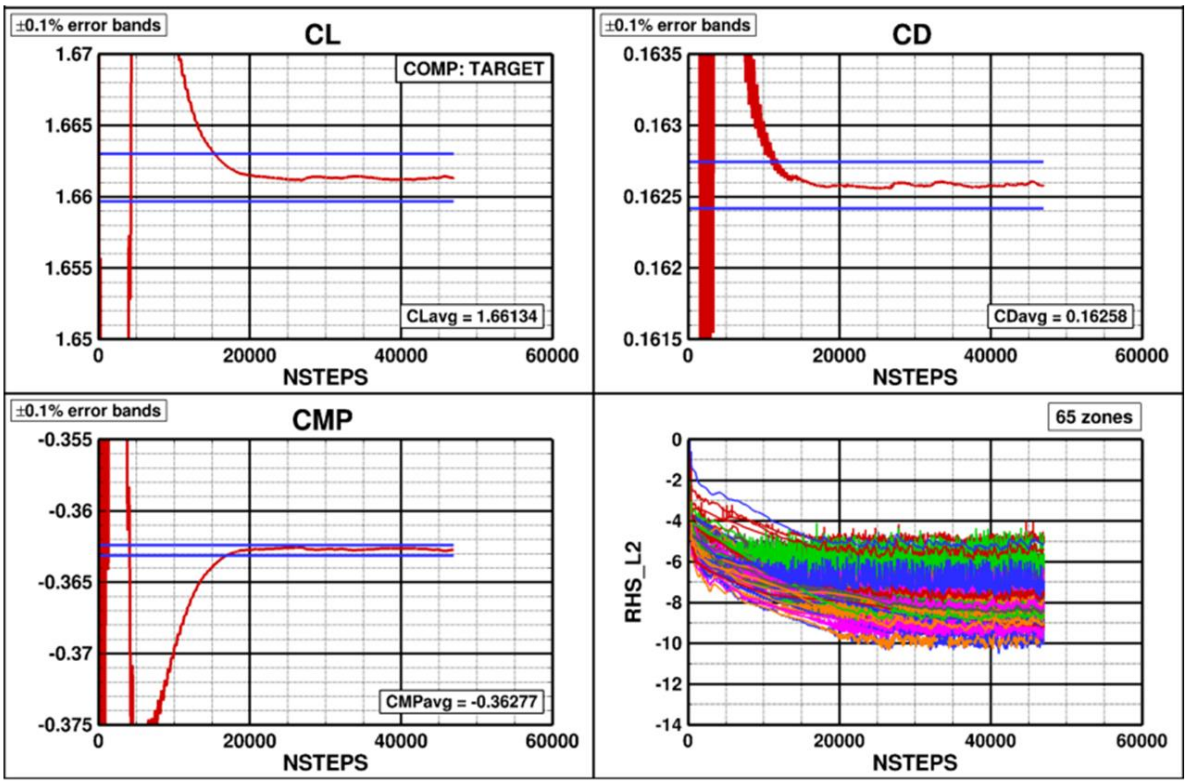

Figure 18. Force, moment and residual convergence from OVERFLOW.

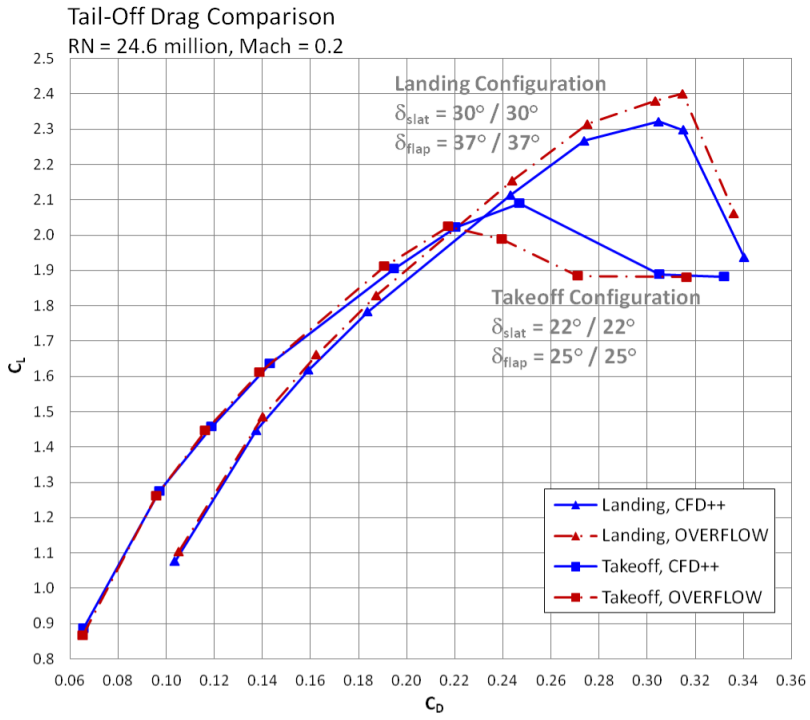

Figure 20. Comparison of takeoff and landing tail-off drag polars from CFD++ and OVERFLOW.

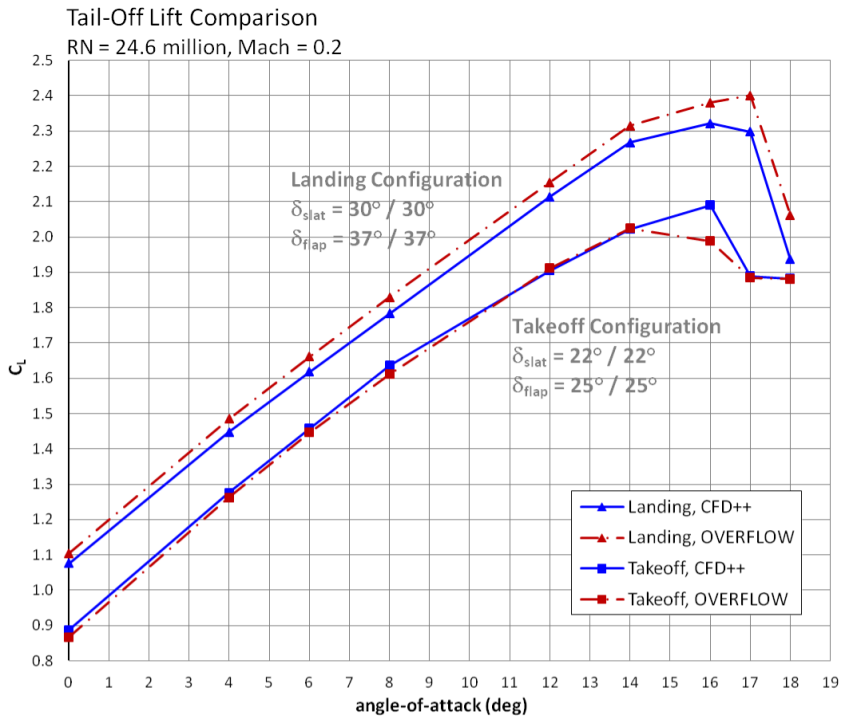

Figure 19. Comparison of takeoff and landing tail-off lift curves from CFD++ and OVERFLOW.

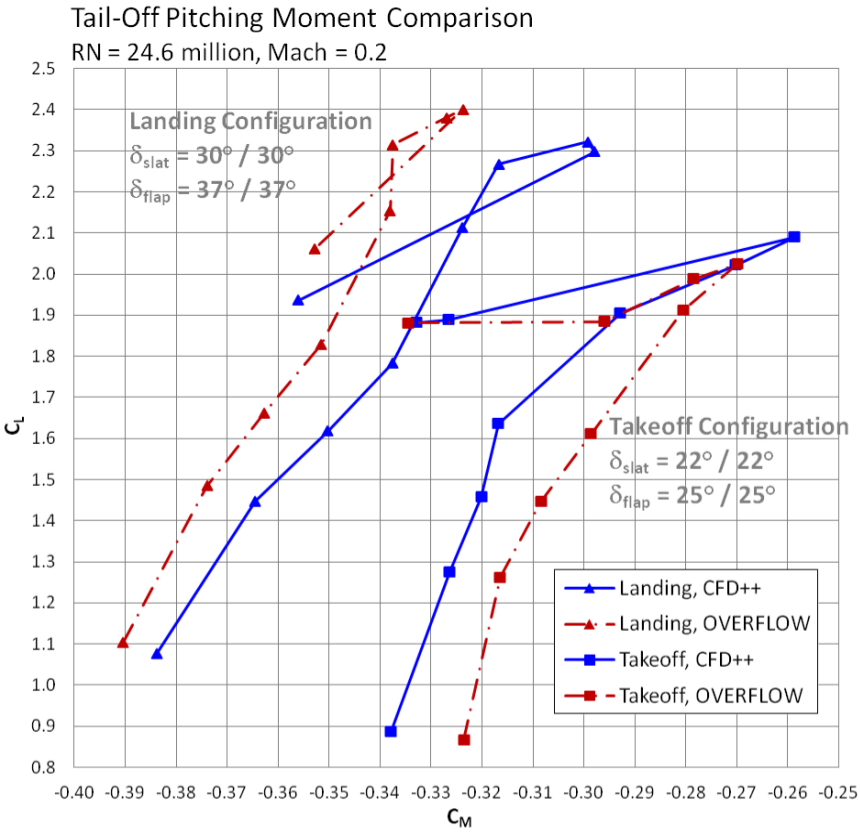

Figure 21. Comparison of takeoff and landing tail-off pitching moment curves from CFD++ and OVERFLOW.

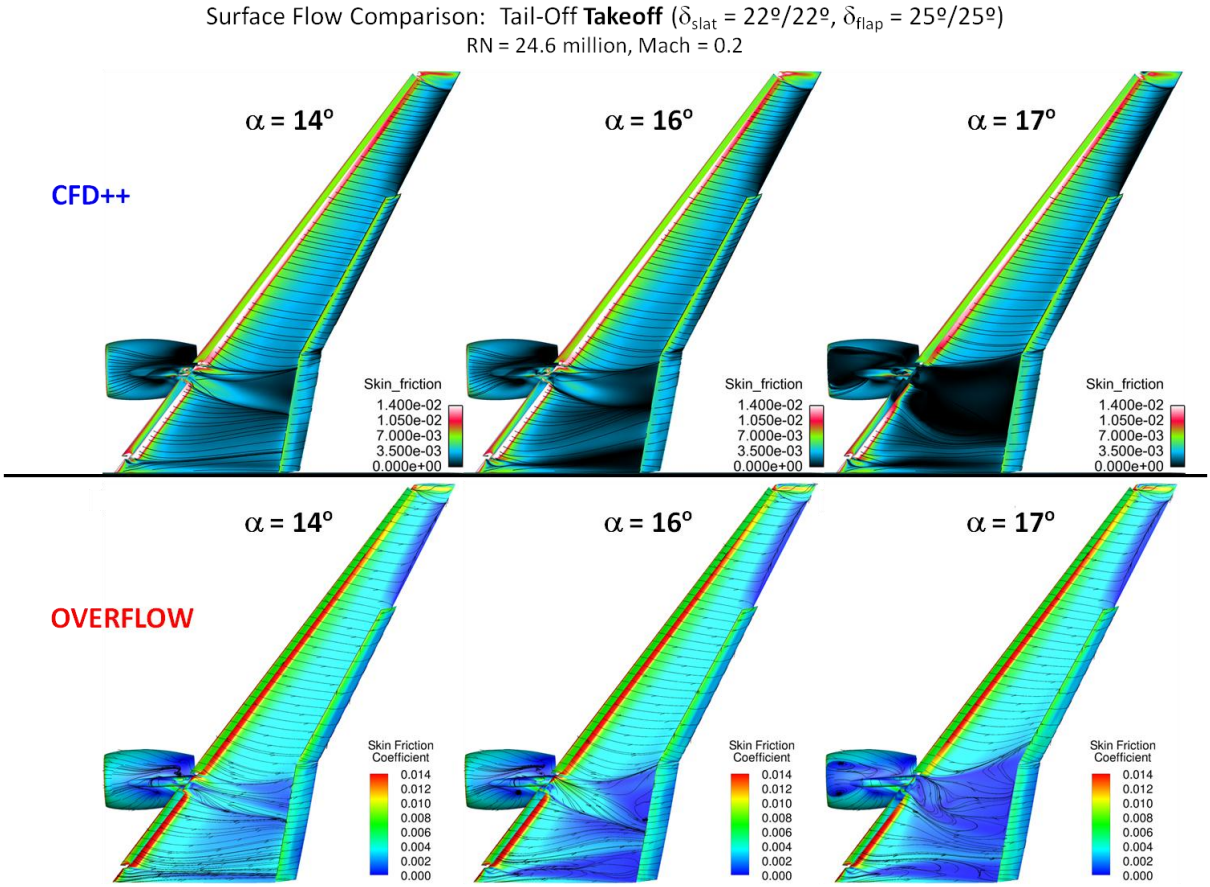

Figure 22. Surface streamlines and skin friction contours for takeoff configuration.

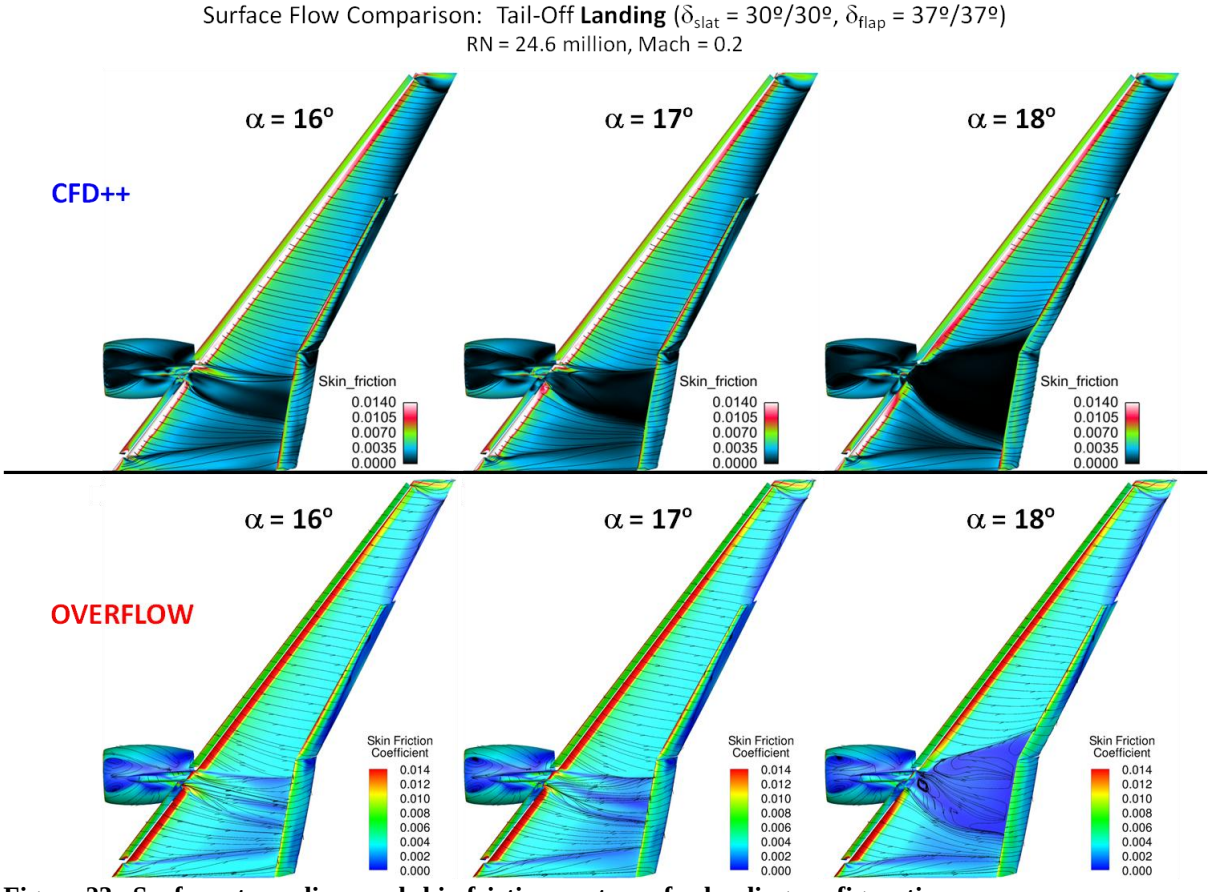

Figure 23. Surface streamlines and skin friction contours for landing configuration.

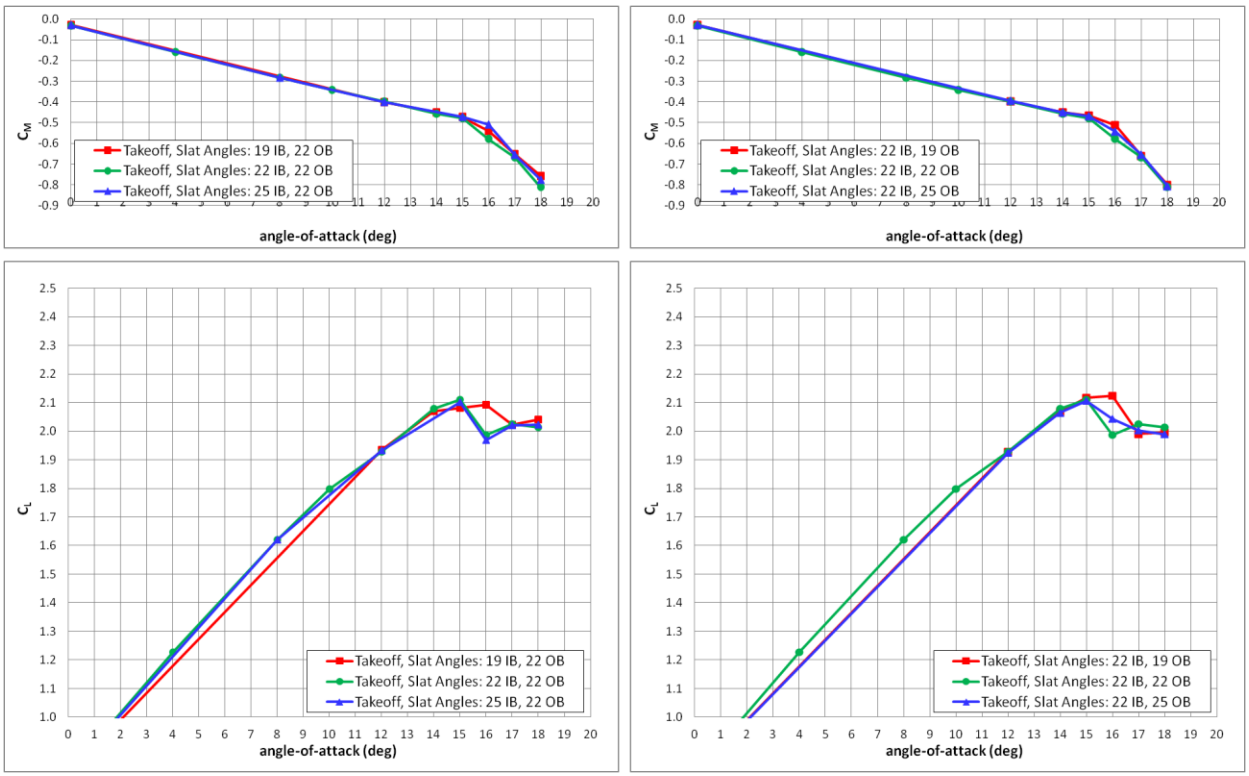

Figure 24. Effect of takeoff slat angle variation from CFD++.

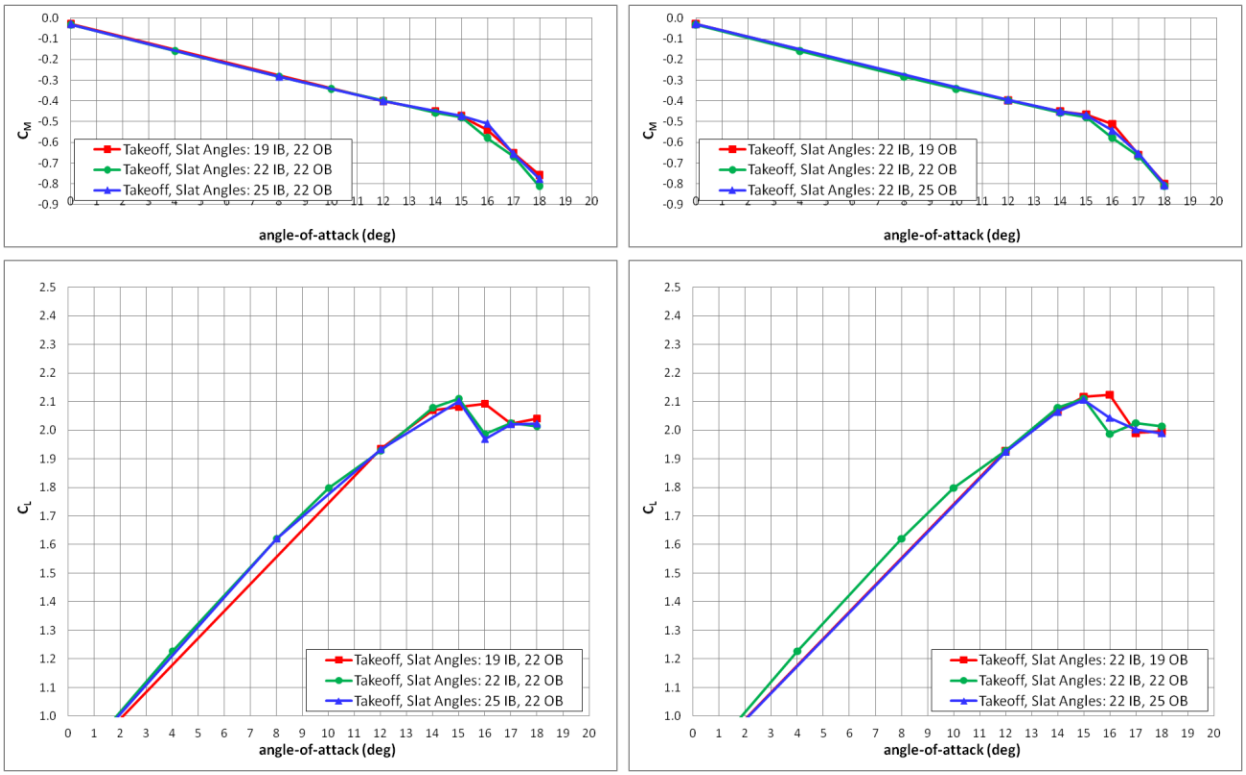

Figure 25. Effect of landing slat angle variation from CFD++.

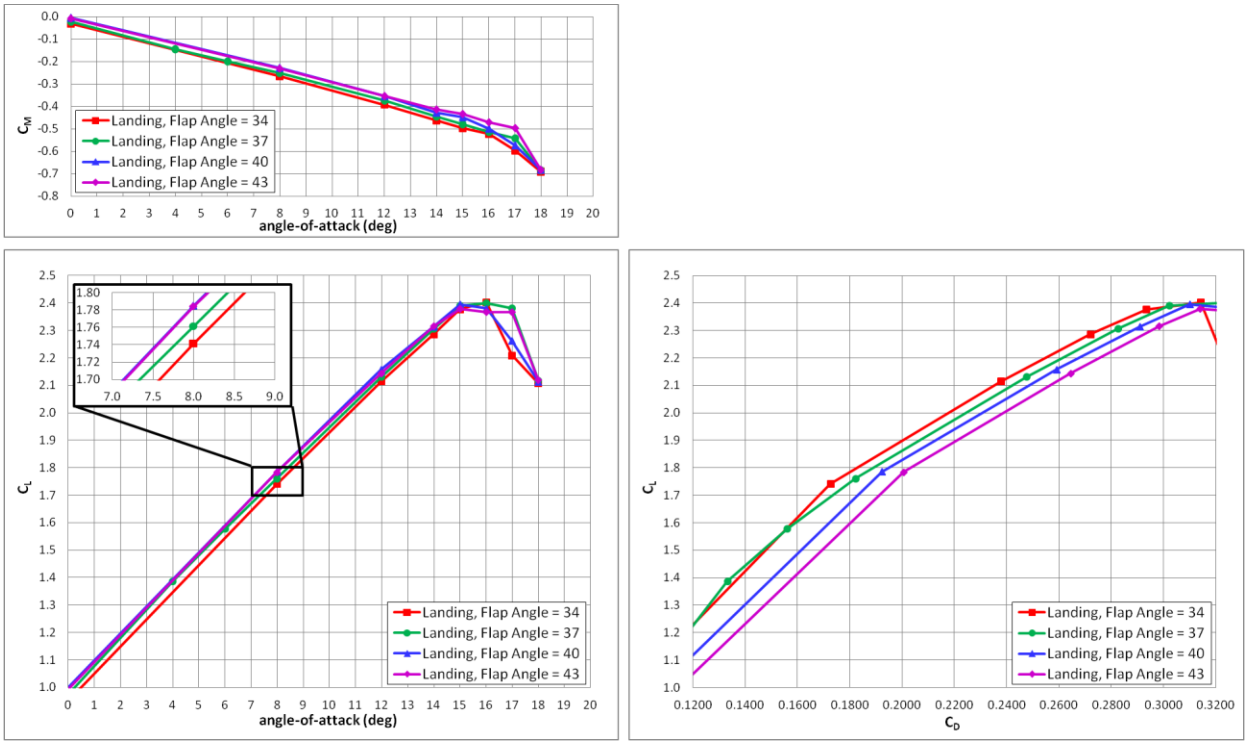

Figure 26. Effect of landing flap angle variation from CFD++.